Intermetallic Phases

Deutsche Ausgabe: DOI: 10.1002/ange.201504315
Internationale Ausgabe: DOI: 10.1002/anie.201504315

# Hybridization Gap and Dresselhaus Spin Splitting in $EuIr_4In_2Ge_4$**

*Nicholas P. Calta, Jino Im, Alexandra P. Rodriguez, Lei Fang, Daniel E. Bugaris, Thomas C. Chasapis, Arthur J. Freeman, and Mercouri G. Kanatzidis**

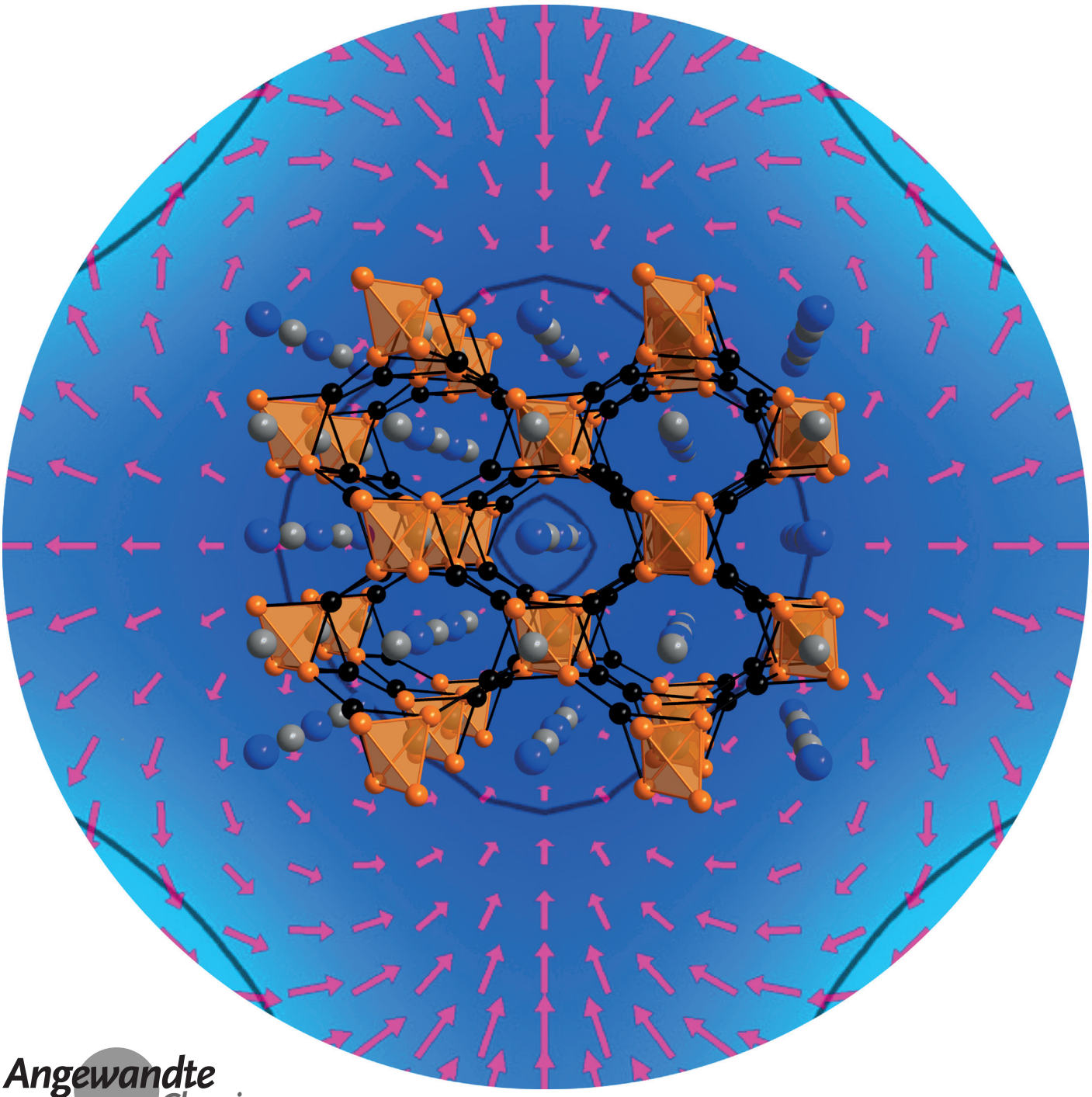

***Abstract:*** *$EuIr_4In_2Ge_4$ is a new intermetallic semiconductor that adopts a non-centrosymmetric structure in the tetragonal $I\bar{4}2m$ space group with unit cell parameters $a = 6.9016(5)$ Å and $c = 8.7153(9)$ Å. The compound features an indirect optical band gap $E_g = 0.26(2)$ eV, and electronic-structure calculations show that the energy gap originates primarily from hybridization of the Ir 5d orbitals, with small contributions from the Ge 4p and In 5p orbitals. The strong spin–orbit coupling arising from the Ir atoms, and the lack of inversion symmetry leads to significant spin splitting, which is described by the Dresselhaus term, at both the conduction- and valence-band edges. The magnetic $Eu^{2+}$ ions present in the structure, which do not play a role in gap formation, order antiferromagnetically at 2.5 K.*

Intermetallic compounds that exhibit semiconducting behavior are rare, and they are of significant experimental and theoretical interest to understand the physics of gap formation. These compounds, broadly known as hybridization-gap materials, exhibit diverse physical properties with band gaps ranging from approximately 0.1 eV in FeSi[1] and $FeSb_2$[2] to 0.5 eV in the half Heusler alloy ZrNiSn.[3] Aside from the wide range of band gaps, reports of enormous Seebeck coefficients as large as $-4500\ \mu V\,K^{-1}$ [4] have driven interest in potential thermoelectric applications for these materials, and some hybridization-gap half Heusler compounds have been predicted to be topological insulators.[5] Hybridization-gap materials exhibit diamagnetic behavior at low temperature with the appearance of thermally activated moments at higher temperature, a further indication of complete pairing of electrons in the conduction and valence bands.[6] The origin of the semiconducting behavior in hybridization-gap compounds depends on the material. Early theoretical explanations for gap formation focused on a d-band Kondo mechanism in analogy with previously known f-based Kondo insulators,[6b] but this hypothesis has largely been replaced by models based on strong, non-Kondo electron correlations.[2b,7] Yet other materials, primarily the half Heusler alloys, have band gaps that form because of strong d–d or d–p bonding, with the valence band completely filled only at a specific electron count.[8] For example, the 0.28 eV indirect band gap in the half Heusler alloy YNiSb arises primarily as a result of d–d band hybridization between the Y and Ni d orbitals caused by bonding between the two.[8b] Furthermore, magnetic f block elements with the appropriate electron count can be introduced into the half Heusler structure without affecting the presence of the band gap, so long as the narrow f band is sufficiently far from the Fermi energy.[9]

In non-centrosymmetric materials with energy gaps exhibiting strong spin–orbit coupling (SOC) effects, the degeneracy of spin-up and spin-down bands can be lifted. This momentum-dependent spin splitting is described by either the Rashba effect,[10] the Dresselhaus effect,[11] or the interplay of both.[12] These effects give rise to rich spin-dependent phenomena and are important in the field of spintronics.[13] Herein, we describe $EuIr_4In_2Ge_4$, a non-centrosymmetric hybridization-gap material exhibiting significant Dresselhaus-type spin splitting and a band gap arising from Ir–Ir bonding similar to the hybridization gaps observed in the Heusler alloys.

$EuIr_4In_2Ge_4$ crystallizes as large, block-like single crystals (Figure 1 a) in the non-centrosymmetric space group $I\bar{4}2m$, and single-crystal X-ray diffraction refinement details can be found in Table 1. The structure of $EuIr_4In_2Ge_4$ (Figure 1) is a tetragonal distortion of the relatively rare cubic $Na_3Pt_4Ge_4$ structure type[14] and is closely related to the recently reported superconductor $Ca_3Ir_4Ge_4$.[15] The main feature of this structure is a three-dimensional network of $IrGe_4$ tetrahedra that condense through a face-sharing arrangement into an $[Ir_4]$

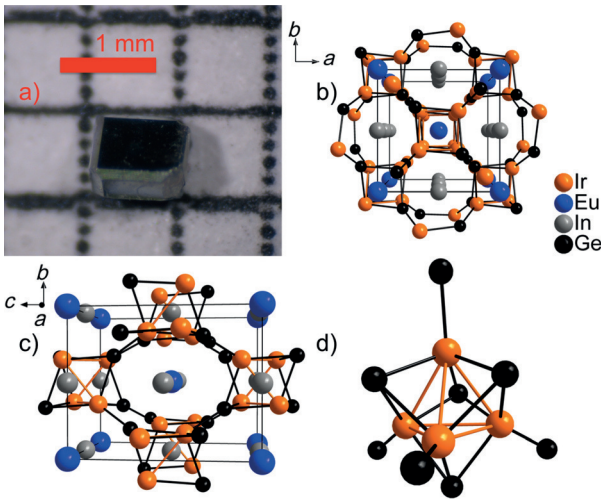


***Figure 1.*** Structure of $EuIr_4In_2Ge_4$ as determined by single-crystal X-ray diffraction. a) Photograph of an as-grown crystal after etching. b, c) Views down the *c* and *a* axes, respectively. d) Distorted $[Ir_4]$ tetrahedron capped by Ge atoms.

[*] N. P. Calta, A. P. Rodriguez, Dr. L. Fang, Dr. T. C. Chasapis, Prof. M. G. Kanatzidis
Department of Chemistry, Northwestern University
2145 Sheridan Rd, Evanston, IL 60208 (USA)
E-mail: m-kanatzidis@northwestern.edu
Dr. J. Im, Prof. A. J. Freeman
Department of Physics, Northwestern University
2145 Sheridan Rd, Evanston, IL 60208 (USA)
Dr. L. Fang, Dr. D. E. Bugaris, Prof. M. G. Kanatzidis
Materials Science Division, Argonne National Laboratory
Argonne, IL 60439 (USA)

[**] We acknowledge the assistance of Prof. Danna Freedman and her research group, as well as support from the Northwestern University's International Institute for Nanotechnology and the State of Illinois Department of Commerce and Economic Opportunity (DCEO) Award (10-203031), which facilitated the magnetic measurements. This work made use of the EPIC facility (NUANCE Center-Northwestern University), which has received support through the MRSEC program (NSF DMR-1121262) at the Materials Research Center, the International Institute for Nanotechnology (IIN), and the State of Illinois, through the IIN. The work at Argonne National Laboratory was supported by the U.S. Department of Energy, Office of Science, Materials Sciences and Engineering. A.P.R. acknowledges support through an Undergraduate Research Grant administered by the Northwestern University Office of Undergraduate Research.

Supporting information for this article is available on the WWW under http://dx.doi.org/10.1002/anie.201504315.

  

***Table 1:*** Single-crystal X-ray diffraction refinement details for $EuIr_4In_2Ge_4$.

| Empirical formula | $EuIr_4In_2Ge_4$ |
|---|---|
| formula weight | 1440.76 |
| temperature [K], wavelength [Å] | 293, 0.71073 |
| space group | $I\bar{4}2m$ |
| unit-cell parameters [Å] | $a = 6.9016(5)$ |
| | $c = 8.7153(9)$ |
| volume [Å$^3$] | 415.13(6) |
| reflections collected, independent | 3848, 619 ($R_{int} = 0.0417$) |
| theta range [°], completeness | 4.68 to 37.96, 99.5 % |
| data/restraints/parameters | 619/0/19 |
| GoF | 1.212 |
| $R$ indices (all data)[a] | $R1 = 0.0188$, $wR2 = 0.0366$ |

[a] $R = \Sigma\,||F_o| - |F_c||/\Sigma|F_o|$, $wR2 = (\Sigma[w(|F_o|^2 - |F_c|^2)^2]/\Sigma[w(|F_o|^4)])^{1/2}$ and $w = 1/[\sigma^2(F_o^2) + (0.0154P)^2 + 5.5965P]$ where $P = (F_o^2 + 2F_c^2)/3$.

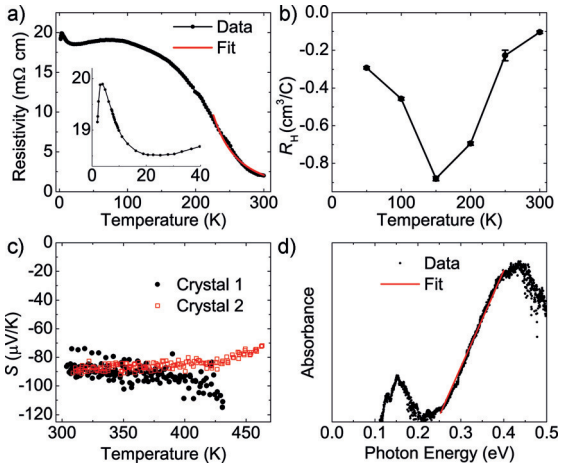


***Figure 2.*** a) Electrical resistivity as a function of temperature on a single-crystal sample. b) The Hall coefficient $R_H$ as a function of temperature. c) The Seebeck coefficient $S$ as a function of temperature for two separate crystals. d) Diffuse-reflectance IR absorption spectrum, indicating an absorption edge at approximately 0.26 eV.

tetrahedron featuring six Ir–Ir bonds and a Ge atom capping each face (Figure 1 d). These cubane-like units share corner Ge atoms, leaving channels between them. In the undistorted parent compound $Ca_3Ir_4Ge_4$, these channels are exclusively occupied by Ca atoms. In $EuIr_4In_2Ge_4$, Eu occupies one third of the Ca positions, and In adopts two thirds in a perfectly ordered manner. To accommodate the substantial difference in size and chemistry between Eu and In, the structure breaks the cubic symmetry of the parent compound through a tetragonal distortion in which Ir–In bonds compress the [$EuIn_2$] channels in the *ab* plane, which is accommodated by the Ir–Ge framework by elongating along the *c* axis. The strong Ir–In bonding also interrupts the channels, effectively isolating the Eu atoms and rendering the structure truly three-dimensional.

$EuIr_4In_2Ge_4$ exhibits semiconducting transport behavior as a result of a hybridization gap with a density of states equal to zero at the Fermi level. The details of transport vary slightly from crystal to crystal owing to extrinsic effects arising from defects, but all measured crystals exhibited n-type semiconducting behavior. In Figure 2 a, a typical zero-field resistivity measurement as a function of temperature with a room-temperature value of 2 mΩ cm is shown. The data have three main features: 1) a region in which the resistivity follows a thermally activated Arrhenius law between 300 K (the highest measured temperature) and roughly 225 K, 2) a distinct shoulder at approximately 200 K leading to nearly temperature-independent resistivity roughly in the range 50–200 K, and 3) a sharp drop below 2.5 K, which is due to magnetic ordering of the $Eu^{2+}$ moments. Features (1) and (3) were present in all measured crystals, whereas (2) was not. Fits to the Arrhenius equation for data from region (1) yield a thermal activation energy value of $E_A = 0.12(1)$ eV. This $E_A$ value is likely a slight overestimate as we did not explicitly determine the contribution from impurity scattering.[16] Nevertheless, the $E_A$ value is smaller than the true band gap ($E_g =$ 0.26(2) eV, described below), indicating that it probably arises from electrons excited from in-gap donor states to the conduction band. The Hall coefficient $R_H$ in the temperature range 50–300 K is shown in Figure 2 b. The $R_H$ coefficient is negative over the entire measured range, indicating electron-type charge carriers. Between 150 K and 300 K, $R_H$ behaves as expected for an n-type semiconductor, increasing as the temperature rises. However, $R_H$ exhibits a minimum at 150 K and decreases with increasing temperature between 50 and 150 K. This unusual minimum in $R_H$ could arise from the interaction of two conduction bands with different carrier masses and mobilities that change position with respect to one another as a function of temperature, a phenomenon that is frequently observed in the valence band of lead chalcogenide salts[17] and other semiconductors with nearly degenerate bands near the band gap.[18]

The Seebeck coefficient ($S$) as a function of temperature between 305 and 470 K is shown in Figure 2 c. The observed value of $S = -90\ \mu V\,K^{-1}$ at 300 K is consistent with an n-type semiconductor and in agreement with the measured $R_H$ value. The $S$ value remained nearly constant until 425 K, at which point it started to become less negative.

In Figure 2 d, we present data from diffuse-reflectance infrared (IR) absorption spectroscopy collected at room temperature under flowing nitrogen. The spectrum shows two clear features: a broad maximum centered at approximately 0.15 eV and an abrupt rise in absorption starting near 0.26 eV. The broad peak at low energy is attributed to thermally excited free carriers present in $EuIr_4In_2Ge_4$ at room temperature. The abrupt rise in absorption corresponds to an optical band gap of 0.26(2) eV, which is larger than the thermally activated in-gap states observed in transport measurements, as expected.

The electronic structure calculated by density functional theory (DFT) confirmed the presence of an energy gap in the density of states. Without SOC, the calculation predicted an indirect band gap of 0.15 eV (Figure 3 a). The projected density of states shown in Figure 3 b reveals that both the conduction band minimum (CBM) and the valence band maximum (VBM) mainly consist of Ir 5d orbitals with small contributions from Ge 4p orbitals and In 5p orbitals. The strong Ir–Ir bonds (2.8069(4) and 3.0796(6) Å) in the [$Ir_4$] tetrahedron are responsible for the existence of the hybrid-

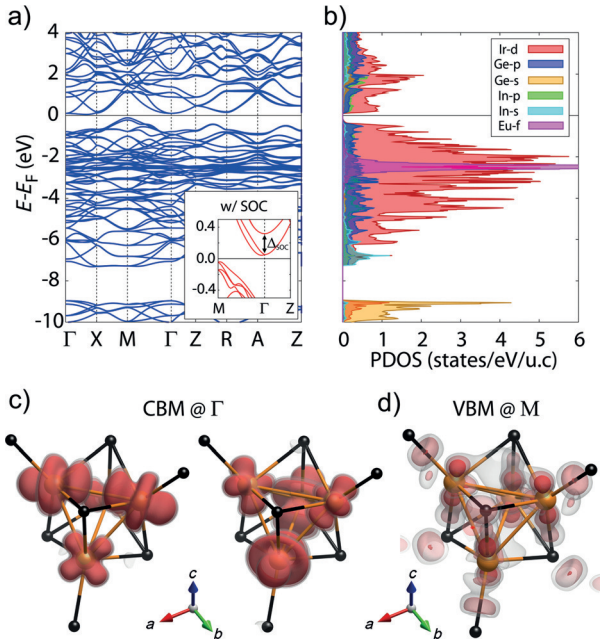


***Figure 3.*** a) Electronic band structure and b) projected density of states (PDOS) of $EuIr_4In_2Ge_4$ without spin–orbit coupling. In both parts, the Fermi level $E_F$ is shown as zero energy. A zoomed-in band structure with spin–orbit coupling (SOC) is depicted in the inset of (a). c) Isosurfaces of the squared wave functions for doubly degenerate CBM states at the Γ point and d) non-degenerate VBM states at the M point. In (c) and (d), orange and black spheres correspond to Ir and Ge atoms, respectively. Isosurfaces are plotted with the same levels in (c) and (d).

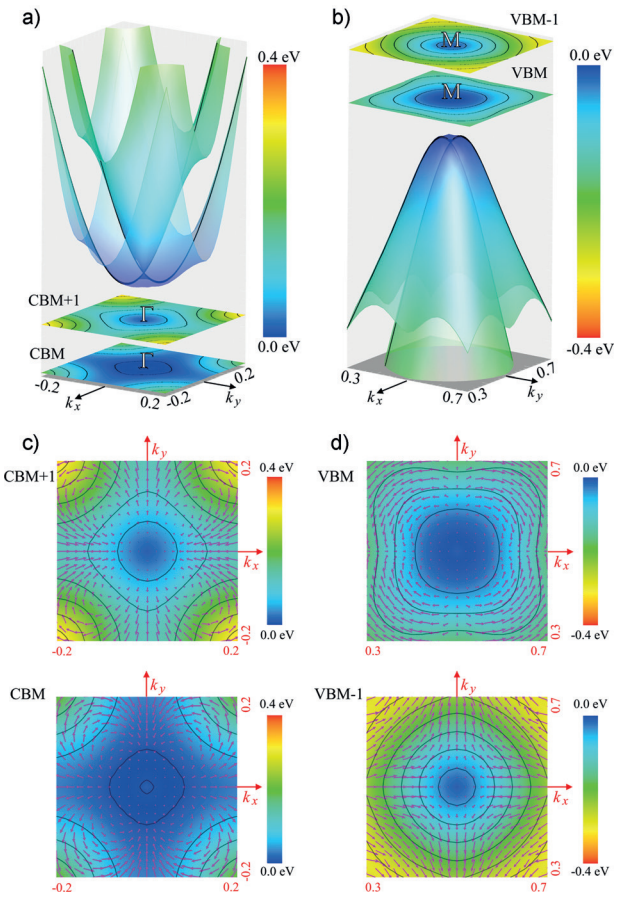


***Figure 4.*** Electronic band structures with SOC for a) the conduction-band edge and the b) valence-band edge presented with a color scheme. Black solid lines are plotted along the M–Γ–M direction in (a) and along the Γ–M–Γ direction in (b). The energy contours of each band are plotted at the bottom of (a) and the top of (b). Spin expectation values are presented for CBM/CBM + 1 in (c) and for VBM/VBM-1 in (d). The same color scheme is employed.

ization gap. Eu f electrons are localized at $E-E_F=-2.5$ eV, and thus do not affect the band structure near the Fermi level. In Figure 3c and d, squared wave functions ($|\psi|^2$) at the Γ and M points show orbital contributions and the band character at the CBM and VBM, respectively. Figure 3c shows two degenerate states at the CBM (Γ point). They are both composite Ir 5d orbitals encompassing the entire [$Ir_4$] tetrahedron and extend primarily in the *ab* plane. These orbitals correspond to molecular E states as a consequence of the $D_{2d}$ point symmetry of the [$Ir_4$] tetrahedron.[19] Figure 3d shows the VBM (M point), a more extended orbital that results from strong hybridization between Ir 5d and Ge 4p states. This delocalized and isotropic orbital character is consistent with the highly dispersive band character of the valence band at the M point.

SOC causes significant modifications of both the conduction- and valence-band edges because of the strong SOC of the Ir atom and the lack of inversion symmetry. SOC has two primary effects on the ground-state electronic structure. First, the doubly degenerate CBM states at the Γ point split into two distinct levels that differ in energy by $\Delta_{SOC}=0.25$ eV. This splitting decreases the size of the indirect band gap of $EuIr_4In_2Ge_4$ by 0.075 eV. Second, the inversion asymmetry in the presence of SOC lifts the spin degeneracy at the valence- and conduction-band edges and leads to momentum-dependent spin splitting. Figure 4a and b present the band splitting as a consequence of the interaction of SOC and the inversion asymmetry at the CBM and VBM, respectively. The energy contours (bottom of 4a, top of 4b) indicate that the CBM states are much more anisotropic than the VBM states, as expected based on the orbital shapes shown in Figure 3c and d.

In the general case, momentum-dependent spin splitting originates either from a Rashba term, a Dresselhaus term, or a combination of the two. However, in a nonpolar crystal lattice, such as the $D_{2d}$ symmetric structure observed for $EuIr_4In_2Ge_4$, only the Dresselhaus term is allowed.[20] The Dresselhaus Hamiltonian is given by:

$$H_D=\beta\left(k_x\sigma_x-k_y\sigma_y\right)+\gamma\left(k_y^2k_x\sigma_x-k_x^2k_y\sigma_y\right) \quad (1)$$

where $k_i$ is the crystal momentum and $\sigma_i$ the Pauli matrix. The coefficients for the linear and cubic terms ($\beta$ and $\gamma$, respectively) are constants defined for each band. Calculations of the spin expectation values $^1/_2(\langle\sigma_x\rangle, \langle\sigma_y\rangle, \langle\sigma_z\rangle)$ yield the spin direction as a function of momentum and reveal spin textures of a given band, allowing us to assess the momentum-dependent spin polarization caused by Dresselhaus terms.

These spin textures are plotted in Figure 4c and 4d for CBM and CBM+1 and VBM and VBM−1, respectively. The VBM−1 state in the lower panel of Figure 4d exhibits the characteristic spin texture for linear Dresselhaus splitting, indicating that the linear term dominates. For the other three displayed orbitals (VBM, CBM, and CBM+1), the spin texture is more complicated with the magnitude of the spin changing as a function of $k$, a signature of the cubic Dresselhaus term. However, the cubic term alone leads to vanishing spin along [100] and [010].[21] As we observed non-zero spin along these two axes, we concluded that both the linear and cubic terms are significant for these three bands. Quantitative evaluations of the $\beta$ and $\gamma$ terms are beyond the scope of this study, but will be important for a more thorough theoretical understanding of $EuIr_4In_2Ge_4$.

Temperature-dependent magnetization measurements taken on an oriented single crystal indicate an antiferromagnetic ordering transition of the $Eu^{2+}$ moments at 2.5 K while Ir carries no magnetic moment. The magnetization data follow a modified Curie–Weiss law above 50 K with a small, negative temperature-independent term $\chi_0$, which is consistent with the diamagnetism expected for hybridization-gap semiconductors. Data plots and fit details are given in the Supporting Information.

In conclusion, $EuIr_4In_2Ge_4$ is a new intermetallic compound with a band gap and significant Dresselhaus-type spin splitting. The combination of these novel features arises from the lack of inversion symmetry and the strong SOC of Ir. The $Eu^{2+}$ magnetic moments present in the structure do not participate in band-gap formation and order antiferromagnetically below 2.5 K. $EuIr_4In_2Ge_4$ adopts a new modification of a rare structure type that contains [$Ir_4$] clusters with strong Ir–Ir bonding. $EuIr_4In_2Ge_4$ may be the first of a new family of hybridization-gap compounds similar to the half Heusler alloys. For this reason, we believe that $EuIr_4In_2Ge_4$ and related compounds with the same structure type merit further experimental and theoretical investigations as a platform for exploring the interplay of hybridization physics and spin splitting.

## Experimental Section

Synthesis: Eu (Chinese Rare Earth Information Center, Inner Mongolia, China, 99.9% lump filed to coarse powder shavings in a glove box), Ir (American Elements, 99.95% powder), and Ge (Plasmaterials, 99.999% pieces ground to coarse powder) were added to an alumina crucible in a 1:1:1 ratio with 30 equivalents of In (Plasmaterials, 99.999% pieces). The reactions were conducted on a 0.5 mmol scale with a total mass of 1.931 g. A stainless steel filter and alumina counterweight were placed atop the crucible, and this assembly was then sealed in a fused silica tube under vacuum. The sealed tube was placed in a furnace and heated to 1000 °C for 12 h, soaked at that temperature for 12 h, cooled to 550 °C over 2 days, and then removed from the furnace and quickly centrifuged to remove the flux. Some In remained on the surface of the crystals and was removed by etching in 5% HCl for 24 h followed by mechanical cleaning. This procedure produced a single-phase product with a typical yield of greater than 80% and very large crystals (ca. 2 mm on edge). Some of the particularly large crystals contained small In inclusions. To avoid effects from inclusions interfering with physical-property measurements, crystals that were used for measurements were cleaved to small sizes and screened by single-crystal X-ray diffraction to confirm their identity and quality. All physical-property measurements were performed on individual single crystals with the exception of infrared spectroscopy measurements.

Single-crystal X-ray diffraction data were collected using a STOE IPDS2T diffractometer and reduced with the STOE X-Area software suite.[22] The crystal structure of $EuIr_4In_2Ge_4$ was solved with direct methods and refined with the SHELX programs.[23]

Diffuse-reflectance IR absorption spectra were measured using a Nicolet 6700 spectrometer on powder samples obtained by crushing a few large crystals.

Magnetic measurements were carried out on a Quantum Design MPMS. Data were collected on oriented single crystals contained in a gel capsule and plastic straw. A diamagnetic correction to account for core electrons was applied to the data prior to fitting.

Resistivity and Hall effect measurements were taken using the resistivity attachment of a Quantum Design PPMS. The Seebeck coefficient was measured under vacuum on a home-built system using an MMR sample stage, Keithley model 2182A nanovoltmeter, and a model 6514 electrometer.

The electronic structure of $EuIr_4In_2Ge_4$ was calculated within the density functional theory (DFT) formalism using the projector-augmented wave method[24] implemented in the Vienna Ab initio Simulation Package.[25] The energy cut-off for the plane wave basis was set to 500 eV, and momentum space integrations were performed on a Γ-centered $10\times10\times10$ regular grid. To describe electron exchange and correlation interactions, we employed the generalized gradient approximation (GGA) within the Perdew–Burke–Ernzerhof formalism.[26] To account for the strong on-site Coulomb interaction of Eu f electrons, we used the DFT+U approach with an effective Hubbard parameter, $U_{eff} = U - J = 8.0$ eV.[27] Spin–orbit coupling (SOC) was evaluated using the second-order approximation[28] within a non-collinear scheme. For the band-structure and density-of-states calculations, we adopted an antiferromagnetic ordering configuration of the Eu atoms because it was calculated to be 0.14 meV per atom more stable than a ferromagnetic configuration. This hypothesis is in agreement with the experimental observation of an antiferromagnetic ground state.

**Keywords:** crystal growth · electronic structure · hybridization · intermetallic phases · X-ray diffraction

**How to cite:** *Angew. Chem. Int. Ed.* **2015**, *54*, 9186–9191
*Angew. Chem.* **2015**, *127*, 9318–9323

[1] L. F. Mattheiss, D. R. Hamann, *Phys. Rev. B* **1993**, *47*, 13114–13119.
[2] a) M. S. Figueira, J. Silva-Valencia, R. Franco, *Eur. Phys. J. B* **2012**, *85*, 1–9; b) H. Takahashi, R. Okazaki, I. Terasaki, Y. Yasui, *Phys. Rev. B* **2013**, *88*, 165205.
[3] S. Öğüt, K. M. Rabe, *Phys. Rev. B* **1995**, *51*, 10443–10453.
[4] B. C. Sales, A. F. May, M. A. McGuire, M. B. Stone, D. J. Singh, D. Mandrus, *Phys. Rev. B* **2012**, *86*, 235136.
[5] S. Chadov, X. Qi, J. Kübler, G. H. Fecher, C. Felser, S. C. Zhang, *Nat. Mater.* **2010**, *9*, 541–545.
[6] a) C. Petrovic, J. W. Kim, S. L. Bud'ko, A. I. Goldman, P. C. Canfield, W. Choe, G. J. Miller, *Phys. Rev. B* **2003**, *67*, 155205; b) C. Petrovic, Y. Lee, T. Vogt, N. D. Lazarov, S. L. Bud'ko, P. C. Canfield, *Phys. Rev. B* **2005**, *72*, 045103; c) P. Sun, N. Oeschler, S. Johnsen, B. B. Iversen, F. Steglich, *Phys. Rev. B* **2009**, *79*, 153308; d) M. B. Gamża, J. M. Tomczak, C. Brown, A. Puri, G. Kotliar, M. C. Aronson, *Phys. Rev. B* **2014**, *89*, 195102.
[7] a) M. Klein, D. Zur, D. Menzel, J. Schoenes, K. Doll, J. Röder, F. Reinert, *Phys. Rev. Lett.* **2008**, *101*, 046406; b) J. M. Tomczak, K. Haule, G. Kotliar, *Proc. Natl. Acad. Sci. USA* **2012**, *109*, 3243–3246.

  

[8] a) T. Graf, C. Felser, S. S. P. Parkin, *Prog. Solid State Chem.* **2011**, *39*, 1 – 50; b) P. Larson, S. D. Mahanti, S. Sportouch, M. G. Kanatzidis, *Phys. Rev. B* **1999**, *59*, 15660 – 15668.
[9] K. Gofryk, D. Kaczorowski, T. Plackowski, A. Leithe-Jasper, Y. Grin, *Phys. Rev. B* **2005**, *72*, 094409.
[10] E. I. Rashba, *Sov. Phys. Solid State* **1960**, *2*, 1109 – 1122.
[11] G. Dresselhaus, *Phys. Rev.* **1955**, *100*, 580 – 586.
[12] S. D. Ganichev, L. E. Golub, *Phys. Status Solidi B* **2014**, *251*, 1801 – 1823.
[13] I. Žutić, J. Fabian, S. Das Sarma, *Rev. Mod. Phys.* **2004**, *76*, 323 – 410.
[14] W. Thronberens, H.-U. Schuster, *Z. Naturforsch. B* **1979**, *34*, 781.
[15] F. von Rohr, H. Luo, N. Ni, M. Wörle, R. J. Cava, *Phys. Rev. B* **2014**, *89*, 224504.
[16] E. Conwell, V. F. Weisskopf, *Phys. Rev.* **1950**, *77*, 388 – 390.
[17] a) Y. Pei, X. Shi, A. LaLonde, H. Wang, L. Chen, G. J. Snyder, *Nature* **2011**, *473*, 66 – 69; b) J. Zhao, C. D. Malliakas, N. Appathurai, V. Karlapati, D. Y. Chung, S. Rosenkranz, M. G. Kanatzidis, U. Chatterjee, *arXiv:1404.1807 [cond-mat.mtrl-sci]* **2014**.
[18] a) L. W. Aukerman, R. K. Willardson, *J. Appl. Phys.* **1960**, *31*, 939 – 940; b) R. S. Allgaier, *J. Appl. Phys.* **1965**, *36*, 2429 – 2434.
[19] M. S. Dresselhaus, G. Dresselhaus, A. Jorio, *Group Theory: Application to the Physics of Condensed Matter*, Springer, Heidelberg, **2008**.
[20] X. Zhang, Q. Liu, J.-W. Luo, A. J. Freeman, A. Zunger, *Nat. Phys.* **2014**, *10*, 387 – 393.
[21] M. Studer, M. P. Walser, S. Baer, H. Rusterholz, S. Schön, D. Schuh, W. Wegscheider, K. Ensslin, G. Salis, *Phys. Rev. B* **2010**, *82*, 235320.
[22] *X-AREA Version 1.39* **2006**, STOE & Cie GmbH; Darmstadt.
[23] G. Sheldrick, *Acta Crystallogr. Sect. A* **2008**, *64*, 112 – 122.
[24] P. E. Blöchl, *Phys. Rev. B* **1994**, *50*, 17953 – 17979.
[25] G. Kresse, J. Furthmüller, *Phys. Rev. B* **1996**, *54*, 11169 – 11186.
[26] J. P. Perdew, K. Burke, M. Ernzerhof, *Phys. Rev. Lett.* **1996**, *77*, 3865 – 3868.
[27] A. I. Liechtenstein, V. I. Anisimov, J. Zaanen, *Phys. Rev. B* **1995**, *52*, R5467 – R5470.
[28] Y.-S. Kim, K. Hummer, G. Kresse, *Phys. Rev. B* **2009**, *80*, 035203.

Received: May 12, 2015
Published online: June 25, 2015

  